

Numerical Modelling and Thermal Analysis of a Tube-in-Tube Latent Heat Thermal Energy Storage System

Avin Rwehikiza Adolf¹, Tunde Bello-Ochende¹, Michel De Paepe^{1,2}

1 Department of Mechanical Engineering, University of Cape Town, Cape Town, South Africa

2 Department of Electromechanical, System and Metal Engineering, University of Ghent, Ghent, Belgium

(adolfavin@gmail.com: tunde.bello-ochende@uct.ac.za: michel.depaepe@ugent.be)

ABSTRACT

LHTES systems provide high energy density and management in various applications. This study presents a numerical modelling and thermal analysis of a tube-in-tube LHTES using PCM as the storage medium. A 3D transient heat transfer model based on the enthalpy-porosity method was developed to simulate the coupled processes of conduction, convection, and phase change. A computational model, created with ANSYS FLUENT 2023 R1, was validated against experimental data. The study examined how the initial PCM temperature affects the charging time, heat transfer rate, and energy stored, while maintaining a constant HTF mass flow rate of 234 kg/h and an inlet HTF temperature of 333 K. Increasing the initial PCM temperature was shown to reduce charging time by boosting the initial heat transfer rate and extending the peak thermal response, thereby speeding up early-stage melting. After melting is complete, the heat transfer rate sharply drops to nearly zero. Importantly, while the charging rate varies, the total energy storage capacity remains consistent, with all systems reaching a similar maximum capacity. These results highlight that initial PCM temperature is a vital parameter for enhancing charging kinetics without impacting storage capacity, providing valuable insights for designing efficient TES systems.

Keywords: Latent heat thermal energy storage, Phase change material, Tube-in-tube heat exchanger, Numerical modelling, Enthalpy-porosity method

NONMENCLATURE

Abbreviations

3D	Three Dimensions
CFD	Computational Fluid Dynamics
CSP	Concentrated Solar Power
HTF	Heat Transfer Fluid
HPC	High Performance Computing
LHTES	Latent Heat Thermal Energy Storage
PCM	Phase Change Material
PCMs	Phase Change Materials

TES	Thermal Energy Storage
<i>Symbols</i>	
K	Kelvin
L	Liquid
L _H	Latent Heat
M	Mushy
S	Solid

1.1 Introduction

The global transition towards sustainable energy systems is critically dependent on the development of efficient, reliable, and cost-effective energy storage technologies. TES has emerged as a pivotal solution for balancing the mismatch between energy supply and demand, particularly in applications such as CSP, industrial waste heat recovery, building heating/cooling, and thermal management of electronic systems [1].

Among TES methods, LHTES using PCMs is particularly attractive. Unlike sensible heat storage, which relies on temperature change in the storage medium, LHTES utilises the large amount of energy absorbed or released during a material's phase transition (typically solid-liquid) at a nearly constant temperature [2].

The design of LHTES heat exchangers is complicated by their transient operation during charge/discharge cycles. This time-dependent behaviour renders traditional steady-state design methods like LMTD and ϵ -NTU unsuitable, as these assume constant conditions and properties [3].

PCMs are characterised by their high latent heat of fusion, which is exchanged during cyclical phase changes, most commonly melting and solidification [4]. This mechanism is highly effective for TES applications, as it allows energy to be stored during periods of abundance and discharged during periods of need, as shown in Figure 1.

CFD is often preferred over experimental testing due to its ability to eliminate the need for costly and complex experimental setups, facilitate rapid exploration of

numerous design parameters, and enable safe analysis of system behaviour under hazardous or extreme thermal conditions, the scenarios that may be difficult or unsafe to replicate experimentally [5].

The current body of literature has primarily focused on macroscopic performance indicators, leaving a gap in the detailed understanding of the localised and time-dependent thermal behaviour of PCM during phase

change. This study bridges the gap through numerical modelling and thermal analysis of a tube-in-tube LHTES system using ANSYS FLUENT 2023 R1. It provides deeper insight into how variations of initial PCM temperature influence the spatial progression of the melting front, energy storage and local heat transfer within the PCM during melting. These insights offer a more comprehensive understanding that supports the design of more efficient and reliable TES systems.

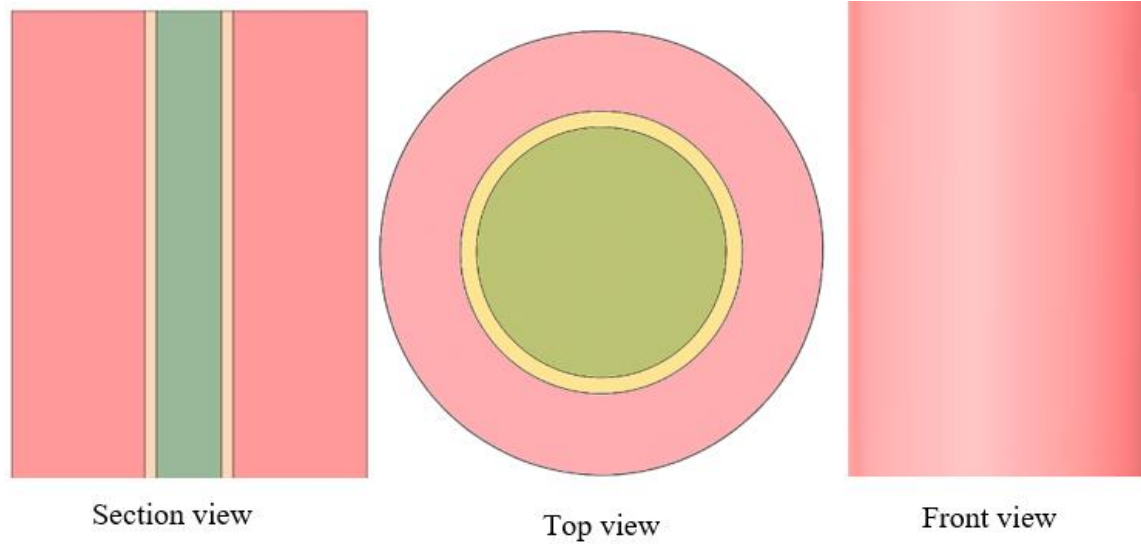


Fig 2: Views of tube-in-tube heat exchangers

1.2 Materials and methods

CFD leverages computer-based simulations and numerical methods to analyse systems involving fluid flow, conjugate heat transfer, and related physical processes. As a mathematical modelling approach, CFD solves the fundamental governing equations, such as conservation of mass, momentum, and energy, to predict the behaviour and performance of the systems. With advances in computing power and the widespread availability of commercial CFD software, these techniques have become essential tools across both industrial and research applications. CFD offers significant advantages by minimising design and testing costs while drastically reducing development timelines [6].

The computational domain is modelled as a cylindrical tube-in-tube heat exchanger, with the inner tube containing HTF and the outer annular region filled with the PCM. Several advantages drive the choice of a cylindrical tube-in-tube configuration: it maintains a uniform cross-sectional area along the height of the exchanger, facilitates effective insulation, enables even

distribution and packing of the PCM, and offers structural integrity due to the circular geometry, which uniformly distributes pressure loads.

The 3D geometry of the heat exchanger was developed using ANSYS FLUENT's SpaceClaim modelling environment, with the dimensions shown in Table 1. The base model design was established using a standard geometry integrated within a tube-in-tube heat exchanger configuration to ensure consistent thermal storage capacity and eliminate discrepancies during the comparative analysis of the LHTES system.

Table 1: Dimensions of the tube-in-tube heat exchanger

Dimension	Copper tube	Polycarbonate tube
Outer diameter (mm)	15	60
Wall thickness (mm)	2	3
Height (m)	1	1

1.3 Theoretical formulation

In the TES system shown in Figure 2, a hot fluid flows through a central pipe, transferring its heat to a PCM

contained in the surrounding outer tube. During charging, the hot fluid flows through the central pipe, releasing heat to the surrounding PCM. This heat absorption melts the PCM, thereby storing thermal energy in the system. Conversely, the cooler fluid circulates through the central pipe, absorbing heat from the PCM as it solidifies, thereby recovering the stored thermal energy. Initially, heat is transferred through conduction, with the PCM nearest to the inner tube's surface melting first as it absorbs thermal energy from the HTF. As melting progresses, variations in temperature cause density differences that generate buoyancy-driven flows. This natural convection enhances the distribution of thermal energy throughout the PCM [7].

The enthalpy method models energy conservation based on temperature-dependent total volumetric enthalpy. It accounts for both sensible heat transfer and the latent heat effect during transformation. This approach offers significant benefits in handling the intricate dynamics of the phase transition interface [8]. Equation 3.5 expresses the general form of the energy equation under constant thermophysical properties. Volumetric enthalpy of PCM integrates both sensible and latent heat components, providing a comprehensive characterisation of TES capacity across all phase transition stages. The formulation gives a robust framework for modelling energy conservation in PCM-based thermal systems [9], [10]. The comprehensive expression representing the total volumetric enthalpy is given in Equation 1.

$$\mathbf{H} = \mathbf{S}_H + m_{PCM}fL_H \quad (1)$$

The sensible volumetric enthalpy represents the portion of thermal energy stored due to temperature changes without phase transition [9]. It is mathematically defined in Equation 2.

$$\mathbf{S}_H = m_{PCM}C_p(T - T_m) \quad (2)$$

The liquid fraction during isothermal phase transformation is commonly modelled using a piecewise function. This function assumes a sharp transition near the melting temperature [11] as expressed in Equation 3.

$$f = \begin{cases} 0 & \text{for } T < T_m \\ \frac{T-T_m}{T_l-T_m} & \text{for } T_m \leq T \leq T_l \\ 1 & \text{for } T_l < T \end{cases} \quad (3)$$

Based on Equations 1-3, the total enthalpy of PCM can be formulated across different temperature intervals, specifically in solid, mushy, and liquid states, by incorporating both sensible and latent heat components [9], as expressed in Equation (3.17).

$$\mathbf{H} = \begin{cases} m_{PCM}C_{p,s}(T - T_m) & \text{for } T < T_m \text{ (S)} \\ m_{PCM}fL_H & \text{for } T_m \leq T \leq T_l \text{ (M)} \\ m_{PCM}C_{p,l}(T_l - T_m) + m_{PCM}L_H & \text{for } T_l < T \text{ (L)} \end{cases} \quad (4)$$

As outlined by [9], an alternative form of the energy conservation equation applicable to 3D heat transfer in both the PCM and the heat exchanger container is provided in Equations 3.18 and 3.19. This formulation enables the accurate simulation of thermal behaviour by accounting for temperature-dependent energy variation across the PCM domain and the heat exchanger walls.

$$\frac{\partial \mathbf{H}}{\partial T} = \frac{\partial}{\partial x} \left(\alpha \frac{\partial \mathbf{H}}{\partial x} \right) + \frac{\partial}{\partial y} \left(\alpha \frac{\partial \mathbf{H}}{\partial y} \right) + \frac{\partial}{\partial z} \left(\alpha \frac{\partial \mathbf{H}}{\partial z} \right) - m_{PCM}L_H \frac{\partial f}{\partial t} \quad (5)$$

$$\frac{\partial \mathbf{H}_f}{\partial T} = \frac{\partial}{\partial x} \left(\alpha_f \frac{\partial \mathbf{H}}{\partial x} \right) + \frac{\partial}{\partial y} \left(\alpha_f \frac{\partial \mathbf{H}}{\partial y} \right) + \frac{\partial}{\partial z} \left(\alpha_f \frac{\partial \mathbf{H}}{\partial z} \right) \quad (6)$$

1.4 Grid refinement test

A grid refinement was conducted by simulating multiple mesh resolutions at an inlet temperature of 333 K. The results, compared systematically in Table 2, confirm that the solution is independent of the discretisation. Based on this analysis, a mesh with a 4 mm element size was chosen for the subsequent heat transfer analysis, as it provided an optimal balance between accuracy, simulation efficiency, and cost-effectiveness.

Table 2: Grid refinement result

Element size (mm)	Element	Node	PCM temp. (K)	Liquid fraction
2	717,432	742,458	333	1
3	222,037	233,286	332	0.9895
4	113,715	120,406	332	0.9891
5	69,901	74,400	330	0.9633
6	56,134	59,274	329	0.9264

1.5 Time step refinement test

A time step refinement was conducted using increments shown in Table 3 to ensure temporal accuracy of the simulation. It revealed that the 0.05s case produced the highest PCM temperature and slightly faster liquid fraction evolution compared to the other time steps. This indicates that the 0.05s interval effectively captured the transient heat transfer and melting dynamics without introducing numerical instability. Hence, the 0.05s time step was selected as the most suitable for subsequent simulations.

Table 3: Time steps refinement result

Time steps (s)	Liquid fraction	PCM Temp. (K)
0.02	0.9890	331.7436
0.03	0.9893	331.7494
0.04	0.9891	331.7636
0.05	0.9894	331.7854
0.06	0.9890	331.7643

1.6 Numerical validity

The comparison between the numerical model of the present study and the experimental data by [12] show a good overall agreement, with both curves exhibiting the characteristic S-shaped melting front over time. This trend, shown in Figure 3, reflects the three distinct melting stages of the PCM: a slow initial phase dominated by sensible heating, a rapid middle phase driven by latent heat absorption and strong convection, and a final phase of reduced melting rate as the system approaches thermal equilibrium. The numerical model slightly overpredicts the melting front position by 0.15 m, which can be attributed to idealised boundary conditions and the assumption of uniform thermal properties in the simulation. Nonetheless, the consistent S-shape behaviour confirms that the model reliably captures the transient heat transfer and phase change mechanisms observed experimentally.

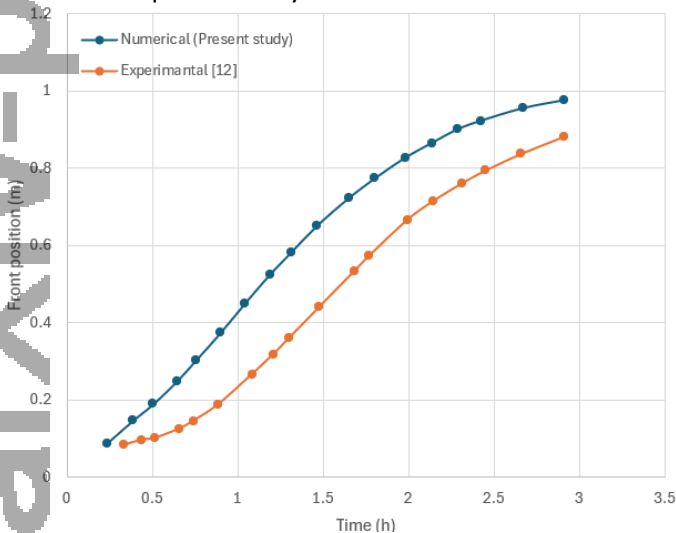


Figure 3: Experimental data by [12] and numerical model, front position (m) against time (h)

1.7 Results and Discussion

The effect of different initial PCM temperatures (284 K, 289 K, 294 K, 299 K, and 304 K) on the melting front, heat transfer rate, and energy stored is discussed under constant HTF mass flow rate (234 kg/h) and inlet HTF

temperature (333 K). As shown in Figure 3, the PCM, with a higher initial temperature (304 K), reached the full melting front position faster than at lower temperatures (284 K). This is because less sensible heat is required to raise the PCM to its melting point. This trend indicates that melting progresses more slowly in its early stages at lower initial temperatures, owing to the higher energy required to reach the fusion point. With an increase in initial temperature, the curves shift upward, signifying both an earlier onset of melting and a faster propagation of the melting front. These results imply that higher initial PCM temperatures enhance thermal responsiveness and shorten melting duration.

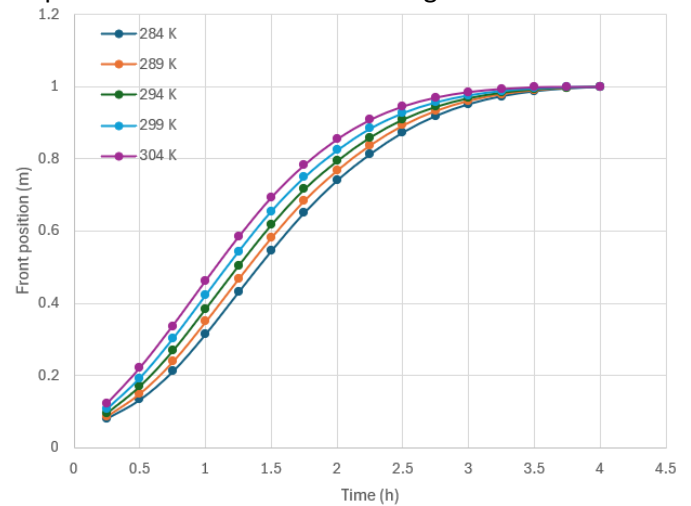


Fig 3: Observation of the effect of different initial PCM temperatures on the melting front (HTF mass flow rate = 234 kg/h, HTF inlet temperature = 333 K)

As shown in Figure 4, the heat transfer rate increases sharply for all initial PCM temperatures due to the high temperature difference between HTF and the solid PCM. PCM, with a higher initial temperature, exhibits a slightly higher initial heat transfer rate because less energy is needed to reach the melting point. The heat transfer rate peaks during melting before decreasing as the absorption of latent heat dominates the process. PCM, with a higher initial temperature, maintains peak rate longer and at a slightly higher level, leading to faster melting. Consequently, the heat transfer rate drops sharply to nearly zero once melting occurs, as the temperature difference between the HTF and PCM diminishes.

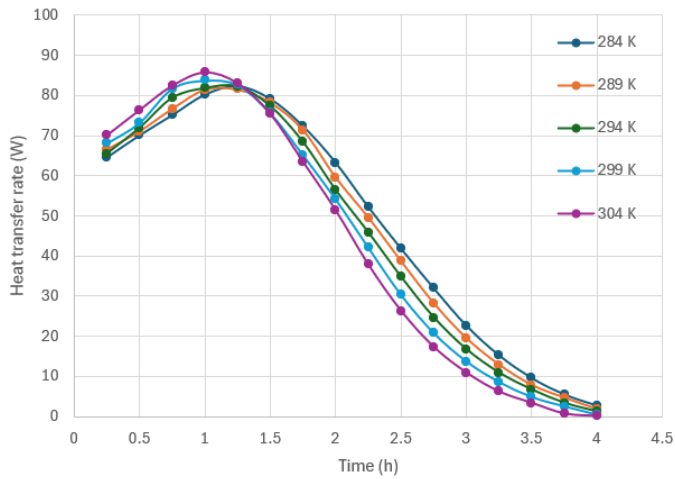


Fig 4: Variation of heat transfer rate for different initial PCM temperatures (HTF mass flow rate = 234 kg/h, HTF inlet temperature = 333 K)

The results in Figure 5 indicate that a higher initial PCM temperature enhances the energy storage rate during the initial charging period and throughout the melting phase. This is attributed to a lower sensible heat demand before melting begins. All curves converge to a similar maximum storage capacity, revealing that the initial PCM temperature affects the charging rate but not the total energy storage potential.

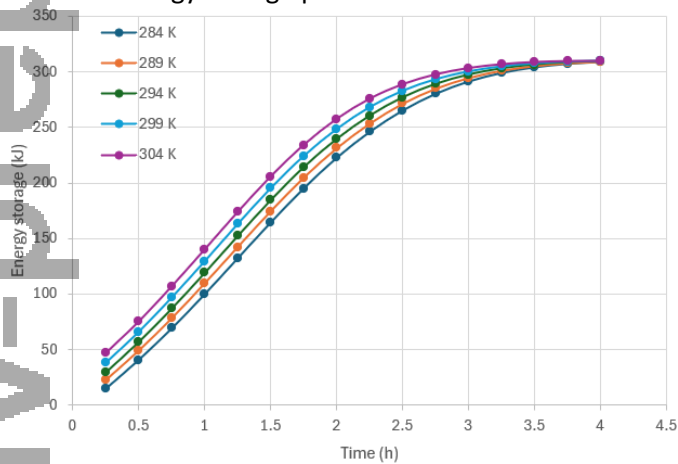


Fig 5: Energy storage performance of the PCM at different initial PCM temperatures (HTF mass flow rate = 234 kg/h, HTF inlet temperature = 333 K)

1.8 Conclusions

The observed trend differs from most previous studies, which mainly examined factors such as the HTF inlet temperature, flow rate, or geometric configuration while assuming a uniform initial PCM temperature significantly below the melting point. The present results reveal that increasing the initial PCM temperature reduces charging time by enhancing the early-stage heat transfer rate and sustaining a higher peak thermal response, which accelerates melting. After complete melting, the heat transfer rate declines sharply, while the total energy storage capacity remains unaffected across

all cases. This finding provides a valuable insight into the transient behaviour of PCM systems, indicating that preheating the PCM can significantly improve charging speed and thermal responsiveness. Thus, identifying the initial PCM temperature as a key factor in enhancing charging kinetics without altering storage capacity provides a practical and effective approach for enhancing TES system performance, especially under time-constrained operating conditions.

1.9 References

- [1] R. Zhu, G. Wei, M. Xu, and G. Wang, "Numerical heat transfer enhancement study on phase change thermal energy storage exchanger with perforated fins," *Int J Heat Fluid Flow*, vol. 115, Sep. 2025, doi: 10.1016/j.ijheatfluidflow.2025.109861.
- [2] H. Zhang, J. Baeyens, G. Cáceres, J. Degrève, and Y. Lv, "Thermal energy storage: Recent developments and practical aspects," Mar. 01, 2016, Elsevier Ltd. doi: 10.1016/j.pecs.2015.10.003.
- [3] W. Beyne, K. Couvreur, I. T' Jollyn, R. Tassenoy, S. Lecompte, and M. De Paepe, "A charging time energy fraction method for evaluating the performance of a latent thermal energy storage heat exchanger," *Appl Therm Eng*, vol. 195, Aug. 2021, doi: 10.1016/j.applthermaleng.2021.117068.
- [4] H. Pointner and W. D. Steinmann, "Experimental demonstration of an active latent heat storage concept," *Appl Energy*, vol. 168, pp. 661–671, Apr. 2016, doi: 10.1016/j.apenergy.2016.01.113.
- [5] F. Agyenim, N. Hewitt, P. Eames, and M. Smyth, "A review of materials, heat transfer and phase change problem formulation for latent heat thermal energy storage systems (LHTESS)," Feb. 2010. doi: 10.1016/j.rser.2009.10.015.
- [6] V. Udoewa and V. Kumar, "Computational Fluid Dynamics," in *Applied Computational Fluid Dynamics*, InTech, 2012. doi: 10.5772/28614.
- [7] Y. Zheng and Z. Wang, "Study on the heat transfer characteristics of a shell-and-tube phase change energy storage heat exchanger," in *Energy Procedia*, Elsevier Ltd, 2019, pp. 4402–4409. doi: 10.1016/j.egypro.2019.01.777.
- [8] V. R. Voller and C. R. Swaminathan, "General source-based method for

solidification phase change,” Numerical Heat Transfer, Part B: Fundamentals, vol. 19, no. 2, pp. 175–189, Jan. 1991, doi: 10.1080/10407799108944962.

- [9] I. Sarbu and A. Dorca, “Review on heat transfer analysis in thermal energy storage using latent heat storage systems and phase change materials,” Jan. 01, 2019, John Wiley and Sons Ltd. doi: 10.1002/er.4196.
- [10] K. Faraj, M. Khaled, J. Faraj, F. Hachem, and C. Castelain, “A review on phase change materials for thermal energy storage in buildings: Heating and hybrid applications,” J Energy Storage, p. 101913, 2021, doi: 10.1016/j.est.2020.101913.
- [11] Y. Hu, K. Zhang, J. Wang, K. Song, L. Wang, and G. Shi, “Thermal performance of cascaded latent heat thermal energy storage units constructed based on solid-liquid interface information,” International Communications in Heat and Mass Transfer, vol. 158, Nov. 2024, doi: 10.1016/j.icheatmasstransfer.2024.107929.
- [12] M. Goderis, J. Van Zele, K. Couvreur, W. Beyne, and M. De Paepe, “Phase change front tracking methods in a vertical tube-in-tube phase change material heat exchanger,” J Energy Storage, vol. 92, Jul. 2024, doi: 10.1016/j.est.2024.112053.

ACKNOWLEDGEMENT

The authors extend sincere gratitude to the Mastercard Foundation Scholars Program for their generous financial support.

The authors acknowledge, with gratitude, the use of the HPC facility at the University of Cape Town, which was instrumental in conducting the simulations for this study.